

Over 10% Efficient Wide Bandgap CIGSe Solar Cells on Transparent Substrate with Na Pre-Deposition Treatment

Mohamed Ould Salem^{1,}, Robert Fonoll¹, Sergio Giraldo¹, Yudania Sanchez¹, Marcel Placidi^{1,4}, Victor Izquierdo-Roca¹, Claudia Malerba², Matteo Valentini², Diouldé Sylla¹, Angelica Thomère¹, Dah Ould Ahmedou³, Edgardo Saucedo^{1,4}, Alejandro Pérez-Rodríguez^{1,5}, and Zacharie Jehl Li-Kao^{1,4,*}*

1. Institut de Recerca en Energia de Catalunya (IREC), 1,2^apl., Jardins de les Dones de Negre, 08930 Sant Adrià de Besòs, Barcelona, Spain.
2. ENEA, Casaccia Research Center, via Anguillarese 301, 00123, Roma, Italy.
3. Department of Physics, Faculty of Sciences and Techniques, University of Nouakchott Al Aasriya, 5026, Nouakchott, Mauritania.
4. Departament d'Enginyeria Electrònica, Universitat Politècnica de Catalunya, C/ Jordi Girona 1, 08034 Barcelona, Spain.
5. Departament d'Enginyeria Electrònica i Biomèdica, IN2UB, Universitat de Barcelona, C/ Martí i Franqués 1, 08028 Barcelona, Spain.

E-mail: msalem@irec.cat, zjehl@irec.cat

Keywords: Wide Bandgap CIGSe, Alkaline treatment, transparent substrate, bifacial solar cell, tandem solar cell

Abstract:

With the recent rise of new photovoltaic applications, it becomes necessary for thin film technologies such as Cu(In,Ga)Se₂ to develop specific optoelectronic properties and take advantage of their high degree of tunability. The feasibility of efficient wide bandgap absorbers on transparent conductive oxide substrates is in that context of critical importance. Using an original approach based on a pre-deposition sodium treatment, Cu(In,Ga)Se₂ absorbers fabricated by sputtering and reactive annealing with a Ga to (Ga+In) content over 0.7 and an optical bandgap above 1.4eV are deposited on transparent fluorine-doped tin oxide films, with the insertion of an ultrathin MoSe₂ layer preserving the contact's ohmicity. Different material characterizations are performed, and a thorough Raman analysis of the absorber reveals that the sodium pre-treatment significantly enhances the Ga incorporation into the chalcopyrite matrix, along with markedly improving the film's morphology and crystalline quality. This translates

in a spectacular boost of the photovoltaic performance for the resulting solar cell as compared to a reference device without Na, specifically in the voltage and fill factor. Eventually, an efficiency exceeding 10% is obtained without antireflection coating, a record value bridging the gap with the state of the art on non-transparent substrates.

1. Introduction

Cu(In,Ga)Se₂ (CIGSe) solar cells have steadily improved in the past 4 decades, with a laboratory record efficiency of 23.35%¹ and a proven viability for large scale industrial development.² Along with these impressive achievements, innovative photovoltaic applications and markets are being considered, among which Building Integrated Photovoltaics (BIPV)³ and the Internet of Things (IoT)⁴ are the most promising. Hence, the properties of existing standard solar cells will be, and already are in some respect, finely tuned to deliver the highest performance possible through this new paradigm. Characteristics such as mechanical flexibility, cell lightweightness, spectral absorption tunability and transparency or bifacial properties are highly desirable features, for which thin film technologies such as CIGSe have undeniable assets. The question of substrate transparency is critical in that regard, as it opens the door for both bifacial and semitransparent devices, but also to the realization of low-cost high efficiency tandem solar cells.

The fabrication of high efficiency CIGSe solar cells on transparent substrates is not new, and nearly 2 decades ago, the pioneering work from T. Nakada in Japan⁵ unequivocally demonstrated that the contact ohmicity could be preserved both on indium tin oxide (ITO) and fluorine-doped tin oxide (FTO) substrates by inserting an ultrathin Mo layer at the back interface. Recent reports of bifacial CIGSe solar cells on ZnO also exist albeit with comparatively lower efficiencies.⁶

Wide bandgap CIGSe solar cells, feasible by increasing the amount of Ga, are especially needed for potential applications as a top cell in low-cost tandem devices,⁷ but high Ga-content devices

have been long known to harbor more detrimental deep defects than their high In-content counterparts.^{8,9} More importantly, the large majority of wide bandgap CIGSe absorbers currently reported are fabricated on opaque metallic Mo substrate, defeating the original purpose. Reported efficiencies are in the range of 11.0% for the pure CuGaSe₂ compound,¹⁰ and range from 12% up to nearly 16% for CIGS compounds with 60-70% of gallium and bandgaps of 1.4-1.5eV,¹¹⁻¹³ all these reports being on SLG/Mo substrates. Very few wide bandgap devices have previously been made on transparent substrate, often with efficiencies well under their Mo-substrate counterparts.¹⁴

In this work, we propose to combine transparent FTO substrates and wide bandgap CIGSe absorbers ($E_g \geq 1.4eV$), and fabricate a proof of concept device with an efficiency exceeding 10% without antireflection coating. It is also worth noting that a deposition method based on metallic precursor sputtering and reactive thermal annealing was used, giving these results even more relevance for a fast technology transfer to the industry. Sodium doping is found to be a key parameter in the devices presented here, and in the course of this study, a comparison will be made with a reference sample, without Na. Moreover, the Na incorporation in the film follows an original approach; while post deposition treatment (PDT) by an alkaline fluoride compound became the standard since the landmark publication from A. Tiwari's group in 2013,¹⁵ we instead propose here a pre-deposition treatment (PreDT), by evaporating 15nm of NaF at the surface of the substrate prior to the fabrication of the CIGSe absorber. Glow Discharge Optical Emission Spectroscopy (GDOES) reveals a steep Ga grading with a single slope profile, as opposed to the commonly reported double grading profile.¹⁶ Using Raman spectroscopy, Na-doping is found as a driving parameter enhancing both the general crystalline quality of the films, but also the Ga incorporation in the matrix. From the Scanning Electron Microscopy (SEM) images, a clearly improved back contact is observed in the case of Na doping, and the fitting of the dark JV curves shows a general improvement in the diode parameters of the solar cells with Na-PreDT. A record efficiency of 10.15% for a 1.41eV

bandgap is achieved on SLG/FTO substrate, with a Ga content in the absorber measured at 68% by X-Ray Fluorescence (XRF). This represents an absolute +1.6% increase of the efficiency ascribed to the Na-PreDT. This result is, to the best of our knowledge, the highest reported efficiency for a wide bandgap CIGSe absorber grown on transparent substrate. To conclude this study, a short paragraph detailing improvement pathways will be presented.

2. Results and Discussions

2.1. Material Analysis

The SEM images of the sample #1 (with Na-PreDT) and sample #2 (reference) with a similar magnification are presented **Figure 1**. The morphology of both samples appear similar at first sight; both samples have a decrease in quality toward the back interface and a bilayer aspect is seen with much smaller grains. The back side of the absorber is where a Ga accumulation is expected;¹⁷ those images hint at a possible phase segregation without the possibility to conclude on differences stemming from the presence of sodium. To complement the visual observation, sample #1 and #2 are analyzed by X-Ray Diffraction, with a specific focus on the (112) and (220)/(204) peaks **Figure 2**. A clear difference can now be made between both samples. Without Na, 2 different phases are observed, a feature particularly visible for the (112) peak (Figure 2b) with a Ga-poor and a Ga-rich contribution, indicating a strong inhomogeneity in the incorporation of Ga to the CIGSe matrix. In the presence of Na however, a well defined single peak is observed **Figure 2b**, a result consistent with a more homogeneous material and thus a better Ga incorporation to the CIGSe matrix. A phase segregation may still exist for this sample, but to a level low enough to be below the instrument's resolution. Regarding the (220)/(204) peaks **Figure 2c**, a peak splitting is expected for high Ga content samples due to the c/a axis distortion of the tetragonal structure rather than phase separation,¹⁸ in the case of

sample #1 (with Na PreDT), 2 peaks are indeed observed, along with a much smaller shoulder at 45.55°; the latter could be attributed to a limited phase separation, which was not visible in Figure 2b. For sample #2 however (no Na), 3 well defined peaks are visible, indicating again a clear phase separation between a Ga-poor and a Ga rich layer, much more pronounced than in the presence of Na.

The samples' depth composition is a critical parameter of this study, and specifically the Ga and Na profiles. Using the GDOES analysis presented **Figure 3a** and **Figure 3b**, several remarks can be made. For both sample #1 and #2, a Cu depletion is observed near the front interface, hinting at the presence of an OVC phase though not unequivocally demonstrating it. Both samples exhibit a single Ga grading profile, with a steep accumulation toward the back interface, and without appreciable difference between both samples. Very little differences are observed in the In and Se profiles, a result anticipated as both samples are processed within the same batch. The Na element is as expected present throughout the absorber for samples #1, while the analysis of sample #2 confirms that FTO is an efficient barrier for its diffusion from the SLG substrate. As a general observation, it is interesting to note that no sample shows specific features from an elemental depth composition viewpoint.

Raman spectroscopy is a valuable tool to dwell in the Na-PreDT influence regarding the film properties, and we chose an approach based on 2 excitation wavelengths; a high energy excitation of 325nm extremely sensitive to the samples' surface, and a more standard 532nm excitation allowing a deeper probing of the films. The Raman spectra shown **Figure 4a** and **Figure 4b** are for 325nm and 532nm excitation wavelengths respectively, for sample #1 and sample #2. As explained in the Experimental part of this study, a direct comparison between both excitations should not be made, and only a relative comparison between both samples at a given excitation wavelength is relevant. For both wavelengths, the spectra are characterized by a dominant peak around 180cm⁻¹ followed by smaller contributions. The peak at 180cm⁻¹ is identified with the A1 mode of the Cu(In,Ga)Se₂ in the chalcopyrite structure (space group

I4 $\bar{2}$ d) with a [Ga]/([Ga]+[In]) ratio in the range of the 50-60%, consistent for both excitation wavelengths; ^{19,20} a value slightly lower than determined by XRF, but in line with the expectations, as it was shown that a significant part of the Ga is accumulated at the back side of the films. Additional weak contributions at 195, 223, 242 and 257cm⁻¹ are observed for the 532nm excitation (Figure 4b), and at 146cm⁻¹ for the 325nm excitation specifically (Figure 4a); identifying the origin of these contributions is not trivial. The 195cm⁻¹ contribution can possibly be attributed to the Cu-Au Cu(In,Ga)Se₂ structure (space group P4 \bar{m} 2), showing similitudes with the very copper-poor CuInS₂ case.²¹ This would however be, to our knowledge, the first time that such phase is reported in Ga-rich CIGSe samples, and caution should thus be exercised. The 146cm⁻¹ peak observed under UV conditions only (325nm excitation, Figure 4a) has several possible interpretations. It can firstly be ascribed to a resonant enhancement effect of the Cu(In,Ga)Se₂; however, one should note that it could also be associated with the presence of an OVC rich in Ga.^{22,23} To unequivocally identify the origin of this peak, a more detailed analysis using a known reference samples would be necessary. Finally, the complex structure in the region of the 200-260cm⁻¹, which is visible for both excitations, is associated with the E and B modes of the chalcopyrite structure of CIGSe and their variations are related to the ratio of the Ga/(Ga+In) in the CIGSe solid solution.²⁴ However, the overlapping of the OVC and Cu-Au contributions cannot be discarded.

The comparison of sample #1 and #2 spectra shows that clear differences exist between both. Focusing on Figure 4b (532nm excitation) only, the main peak of the CIGSe is slightly shifted, suggesting a higher Ga ratio in the Na-PreDT samples, possibly 5% to 10% higher. This agrees well with the shift and the relative intensity of the weak peaks in the 220-260cm⁻¹ region observed under 532nm and the similar shift observed under 325nm excitation. As the GDOES analysis showed a similar Ga elemental profile between both samples, this result tends to indicate a better Ga incorporation to the CIGSe matrix in the presence of Na close to the surface. This observation is consistent with previous work on Na doping of CIGSe absorbers.²⁵

Remarkably, the 195cm^{-1} contribution associated with the Cu-Au structure is absent in sample #1 (Na-PreDT sample) under 532nm excitation, while it appears for both samples under 325nm excitation. While the presence of this phase has been associated with a degradation of the devices's performance, previous studies by our group on CuInS_2 device²¹ showed an improvement of the J_{sc} , but a reduction of the V_{oc} , and R_s . This was ascribed to a reduction of the defect concentration in the Cu-poor CuInS_2 by the accumulation of these defects in the more disordered Cu-Au phase, hence allowing a better crystalline quality in the chalcopyrite CuInS_2 . It is unconfirmed if a similar conclusion is applicable here.

Focusing again on 532nm excitation (Figure 4b), the FWHM of the main 180cm^{-1} peak is markedly reduced in sample #1 (from 7.9cm^{-1} to 6.7cm^{-1}). This indicates that the Na-PreDT is associated with an improvement of the crystal quality of the CIGSe, which would be in agreement with the reduction of the Raman contributions of the Cu-Au disordered phase. Finally, a small shoulder in the $155\text{-}165\text{cm}^{-1}$ region is observed in sample #1 (Figure 4b), and it is attributed to the presence of the OVC. This phase allows to accommodate the Cu-poor conditions of the absorber; the order of the defect in the structure allows to obtain an absorber with better optoelectronic properties.²⁶

As a summary of the Raman analysis of the samples, 2 main observations should be kept in mind. The most important one is that Na-PreDT significantly improves the Ga incorporation in the CIGSe structure (by 5% to 10% in our estimation), as shown by the peaks' shift for both excitation wavelengths; and secondly, a possible improvement of the general crystalline quality of the films can also be attributed to the Na-doping, illustrated by the reduced FWHM of the 180cm^{-1} peak in Figure 4b. A similar observation can however not be made in Figure 4a, and this should remain at this point an hypothesis as different interpretations (additional contributions) may exist for this FWHM difference.

2.2. Electrical characterization of devices

Solar cells are fabricated for samples #1 (with Na PreDT) and #2 (no Na) following the previously described standard process and electrically characterized by Current-Voltage analysis (JV) under AM1.5 illumination and dark conditions, and External Quantum Efficiency (EQE).

Figure 5 shows the JV characteristic of sample #1 and #2 along with their respective photovoltaic and diode parameters. A remarkable improvement of the performance is observed for the device with a Na-PreDT; specifically, the Fill Factor jumps from 60.3% to 65.6%, and the V_{oc} is brought from 588mV to 668mV. A similar observation was made in reference ²² regarding the influence of Na on these two parameters. While a slight reduction of the current is observed (from 24.3mA.cm⁻² without PreDT down to 23.2mA.cm⁻² for sample #1), the efficiency is markedly improved and reaches a record value of 10.15%. This value is the main result of this work, and it is to the best of our knowledge the highest reported efficiency for a CIGSe solar cell on transparent substrate with a bandgap larger than 1.4eV, getting close to those obtained with similar absorbers fabricated on metallic Mo substrates. It should also be noted that it was obtained without an antireflection coating, and there still exists a straightforward margin for improvement in that regard. **Table 1** presents an overview of the most relevant contributions in wide bandgap CIGSe solar cells; our device, albeit on transparent substrate, favorably compares with the highest reported values in terms of both efficiency and V_{oc} . The fitting of the dark JV curves using a single diode model reveals that both the shunt resistance and reverse saturation current are improved by the Na-PreDT in sample #1. This observation is consistent with a possibly improved film morphology observed in the Raman analysis Figure 4b. The Na-PreDT, by improving the film's crystallinity, would reduce both the shunt pathways along with the density of recombination centers, the latter being closely related to J_0 ,²⁷ yielding an overall superior diode performance.

The EQE analysis of samples #1 and #2 is presented **Figure 6**, using EQE curves normalized to 1 for relative comparisons between both samples (see experimental part). **A clear difference in the bandgap between both samples is visible, and while the GDOES composition analysis indicated a roughly similar GA profile in the films, such difference comes to no surprise; the XRD analysis indicated a clear phase separation in sample #2 (no Na), with a poor homogeneity in Ga incorporation and thus a Ga-poor phase reducing the bandgap of the absorber. Sample #1 on the other hand exhibited a more homogeneous Ga incorporation, resulting in a material with an overall higher bandgap.** The Raman characterization additionally confirmed this observation that Na-PreDT leads to a better Ga incorporation in the CIGSe. The normalized EQE onset at the vicinity of the bandgap is also steeper for sample #1, an indication of a better collection of charge carriers generated from low energy photons, and thus of an improvement of the back interface's quality of the absorber. **A result consistent with a material with a lower level of phase segregation.**

For a direct bandgap, the absorption coefficient depends on $\alpha h\nu \propto (h\nu - E_g)^{1/2}$. Hence, a plot of $h\nu \times \ln(1 - EQE)^2$ against $h\nu$ gives a reasonable extrapolation of the electronic bandgap E_g , as shown in the inset of Figure 6. Using Na-PreDT, E_g is increased from 1.32eV to 1.41eV, an effect fully attributed to the better and more homogeneous Ga incorporation discussed during the XRD and Raman analysis.

The electrical characterization of our samples demonstrates that the Na-PreDT permits the fabrication of wide bandgap CIGSe solar cells on a transparent substrate with performance rivaling the state of the art on metallic Mo substrate; it is however important to point out that some limitations and improvement pathways remain, which are discussed in the last part of this work.

2.3. Limitations and improvement pathways

The most critical improvement pathway lies in the actual transparency of the back contact. In this work, the MoSe₂ thickness was estimated to be 30-40nm; while still allowing for a certain level of transparency (45% at 700nm in our case, see Supporting Information **Figure S 1**), our recent work on Transition Metal Oxides reveals that the transparency of the back contact can potentially be doubled (Supporting Information **Figure S 2**), though electrical optimizations are still needed to improve the contact's ohmicity.

While beyond the scope of this work, other alkali elements are under evaluations for wide bandgap CIGSe films on FTO, with Rb and Cs being the most promising pathways for further improving the solar cell's performances. Wider bandgaps are also aimed at, with the hope that heavier alkali elements will allow for an even better Ga incorporation in the films. Similarly, a comparison between pre-deposition and the more standard post deposition of the alkali element would bring valuable insights on the species diffusion dynamics and its interplay with the film's morphology. Such study will be combined with an exhaustive defect analysis using a combination of admittance spectroscopy techniques and Raman spectroscopy.

Additionally, this work focused on the improved Ga incorporation when using a Na PreDT, as demonstrated by the XRD/Raman analysis and the bandgap increase; at this point, we do have data to infer other mechanisms through which Na doping would improve the performance of the cells, but such possibility should not be discarded. Additionally, the mechanism of phase separation in the absence of sodium is currently under investigation by our team, with an interplay with the deposition conditions which will be discussed in a future communication.

Finally, the solar cells reported here do not have an antireflection coating. In wide bandgap CIGSe, such layer would provide a significant current bump, and more than 1% of absolute efficiency gain was previously reported from the addition of an ARC.¹⁰ The tested solar cells do not have a metallic grid, and thus could not be certified. While the measurement's

reproducibility is thoroughly assessed during the present study (Supporting Information **Figure S 3**), our future work will focus on improving that specific point for efficiency certification.

3. Conclusion

The work presented here unequivocally demonstrates that wide bandgap CIGSe solar cells can be made with a transparent substrate and retain performances close to the state of the art on metallic non-transparent substrates. With a combination of XRD, GDOES and Raman analysis, we identify the sodium pre-deposition treatment as a key parameter permitting a better and more homogeneous Ga incorporation to the CIGSe film and markedly reducing the phase segregation, resulting in an overall larger bandgap material with improved PV properties. The electrical characterization of complete solar cell devices shows a spectacular performance improvement with the sodium pre-treatment, enhancing both the open-circuit voltage and fill factor of the photodiodes, by way of reducing both the shunts and the recombination parameter J_0 , and resulting in a record efficiency over 10% without antireflection coating. Several improvement pathways are given, and this work represents a proof of concept for efficient wide bandgap CIGSe solar cells with a transparent back contact.

4. Experimental Section

Solar cells fabrication:

The solar cells presented are fabricated with the following material stack:

SLG/FTO/Mo/(NaF)/CIGSe/CdS/ZnO/ITO.

And samples with and without NaF are compared (sample #1 and sample #2).

The SLG/FTO substrate is purchased from Sigma-AldrichTM (reference #735183). A thin Mo layer ($< 15nm$) is deposited by DC sputtering on the substrate, to help with the formation of MoSe₂ during the reactive annealing stage. The Na-PreDT consists in the thermal evaporation

of a 15nm NaF layer for sample #1, while sample #2 is the reference without the NaF layer. It is worth noting that FTO is known to efficiently block the diffusion of Na from the SLG substrate, and we make the assumption that the absorber for sample #2 is Na-free.

For the fabrication of the CIGSe absorber, a Cu-In-Ga metal precursor is deposited by DC magnetron sputtering for the Cu and Ga elements, and by thermal evaporator for the In element. A 2-step reactive annealing under Se atmosphere is performed by placing the metallic precursor samples in a graphite box along with an optimized amount of elemental Se, and the graphite box is inserted in a quartz tubular furnace. In a first step, the temperature is increased from room temperature to 400°C with a 20°C.min⁻¹ increase rate and a constant 1.5 mbar pressure under an Ar flux (pump valve open); the maximum temperature is maintained for 30 minutes. In a second step, the temperature is increased (same rate) to a maximum value of 550°C for 15 minutes, and the pressure is kept at 1 bar (Ar) without an Ar flux (pump valve closed). The samples are let to naturally cool down at the end of the process. Being Cu deficient in general composition, the as-grown films are expected to feature the formation of a Cu(In,Ga)₃Se₅ Ordered Vacancy Compound (OVC) phase at the vicinity of the front interface. XRF data were acquired for each 1.25cm x 2.5cm sample on 9 different positions, and averaged to obtain what is referred in the text as the sample's composition. This analysis reveals ratio of $\frac{Cu}{In+Ga} = 0.7 \pm 0.01$ (CGI) and $\frac{Ga}{In+Ga} = 0.68 \pm 0.01$ (GGI) for both samples, which should correspond to a bandgap of $E_g \sim 1.45eV$.

Prior to the deposition of the CdS buffer layer by Chemical Bath Deposition (CBD), the as-grown samples are etched for 10 minutes in a 2% KCN bath. The window layer is completed with a 50nm i:ZnO layer and a 300nm ITO layer deposited by DC sputtering. Each sample was mechanically scribed with individual solar cells of dimension 3mm × 3mm. While the record efficiencies are reported here, several sets of samples were fabricated and showed a remarkable consistency. The electrical characterization of the samples is performed several times to assess

any possible light soaking effect, without showing significant variations (less than 0.5% in absolute on the same cell). The fitting of the dark JV curves is made using a 1 diode model code developed in-house. The value reported in this work are based on the total area of the cell. The reported EQE are normalized to 1 and should only be used for relative comparisons, as a strong current discrepancy was observed from the integration of the raw curves (related to calibration issues of the equipment). As sample #1 and #2 have a similar front contact, and as the absorption of the cells is limited by the front contact reflectivity, using normalized curves is deemed appropriate to discuss the bandgap shift between both samples and the absorption onset.

Material characterization:

The as-deposited CIGSe films and complete solar cells are observed by Scanning Electron Microscopy (SEM) to assess their morphology. The morphological features presented in the following section are based on the SEM analysis of hundreds of microns (width) in different cross-section preparations to avoid biased results. We chose in this work to present the images of the complete devices in cross-section.

The films are analyzed by X-Ray diffraction (XRD) using a Bruker D8 Advance with a fixed θ of 0.0173° , scanning rate of $0.3^\circ \text{ min}^{-1}$, a step size of 0.010° , and 2θ range from 0 to 100° , using $\text{CuK}\alpha$ radiation ($\lambda_{\text{ave}} = 1.5406 \text{ \AA}$) operating at 40 kV and 40 mA.

Glow Discharge Optical Emission Spectroscopy (GDOES) is used to obtain the relative depth composition of the films, analyzing each element profile by a Horiba Jobin Yvon GD Profiler 2 spectrometer, equipped with an anode diameter of 4 mm and 19 element channels.

Raman spectroscopy using a Horiba Jobin-Yvon FHR640 spectrometer is performed on the bare CIGSe films with a focus on the identification of possible secondary phases and the qualitative evaluation of the crystalline quality. A high energy 325nm excitation is used to provide surface information (penetration depth $< 10\text{nm}$), and a lower energy 532nm excitation is used for a more in-depth assesement of the films (penetration depth $< 60\text{nm}$). In both cases,

the power density is kept below $25\text{W}/\text{cm}^2$ to avoid any substantial heating of the samples. The spectra were acquired on 5 different positions of a $1.25\text{cm} \times 2.5\text{cm}$ sample. It is important to note that these systems have not been previously studied under 325nm excitation, and a direct quantitative spectra comparison between 532 nm and 325nm is thus not possible. Our study will then focus on comparing films with and without the Na-PreDT under a similar excitation wavelength. **To reduce the uncertainty originating from punctual measurements in the Raman spectra, a large spot diameter (of the order of $100\mu\text{m}$) was used, allowing to reduce the impact of the micro-crystalline inhomogeneities. This is performed using a Raman probe specifically developed in our laboratory.**

Acknowledgements

This research was supported by the H2020 Programme under the project INFINITE-CELL (H2020-MSCA-RISE-2017-777968), by the MasterPV project from the SOLARERANET International program (subproject ref. PCI2018-092945Spanish „Agencia Estatal de Investigacion“) by the Spanish Ministry of Science, Innovation and Universities under the WINCOST (ENE2016-80788-C5-1-R) project, and by the European Regional Development Funds (ERDF, FEDER Programa Competitivitat de Catalunya 2007–2013). Authors from IREC and the University of Barcelona belong to the SEMS (Solar Energy Materials and Systems) Consolidated Research Group of the “Generalitat de Catalunya” (Ref. 2017 SGR 862).

ENEA researchers gratefully acknowledge the Italian Ministry of Economic Development for the support received in the framework of the Operating Agreement with ENEA for the Research on the Electric System.

M.P. thanks the Government of Spain for the Ramon y Cajal Fellowship (RYC-2017-23758).

M.O.S. acknowledges the Islamic Development Bank for the financial support.

Z.J.L.K. acknowledges the TecnioSpring Plus program and the Marie Curie Actions for the financial support.

Received: ((will be filled in by the editorial staff))

Revised: ((will be filled in by the editorial staff))

Published online: ((will be filled in by the editorial staff))

References

- (1) Nakamura, M.; Yamaguchi, K.; Kimoto, Y.; Yasaki, Y.; Kato, T.; Sugimoto, H. Cd-Free Cu(In,Ga)(Se,S)₂ Thin-Film Solar Cell With Record Efficiency of 23.35%. *IEEE Journal of Photovoltaics* **2019**, *9* (6), 1863–1867. <https://doi.org/10.1109/JPHOTOV.2019.2937218>.
- (2) Feurer, T.; Reinhard, P.; Avancini, E.; Bissig, B.; Löckinger, J.; Fuchs, P.; Carron, R.; Weiss, T. P.; Perrenoud, J.; Stutterheim, S.; Buecheler, S.; Tiwari, A. N. Progress in Thin Film CIGS Photovoltaics – Research and Development, Manufacturing, and Applications. *Progress in Photovoltaics: Research and Applications* **2017**, *25* (7), 645–667. <https://doi.org/10.1002/pip.2811>.
- (3) Shukla, A. K.; Sudhakar, K.; Baredar, P. Recent Advancement in BIPV Product Technologies: A Review. *Energy and Buildings* **2017**, *140*, 188–195. <https://doi.org/10.1016/j.enbuild.2017.02.015>.
- (4) Mathews, I.; Kantareddy, S. N.; Buonassisi, T.; Peters, I. M. Technology and Market Perspective for Indoor Photovoltaic Cells. *Joule* **2019**.
- (5) Nakada, T.; Hirabayashi, Y.; Tokado, T.; Ohmori, D.; Mise, T. Novel Device Structure for Cu (In, Ga) Se₂ Thin Film Solar Cells Using Transparent Conducting Oxide Back and Front Contacts. *Solar energy* **2004**, *77* (6), 739–747.
- (6) Cavallari, N.; Pattini, F.; Rampino, S.; Annoni, F.; Barozzi, M.; Bronzoni, M.; Gilioli, E.; Gombia, E.; Maragliano, C.; Mazzer, M.; Pepponi, G.; Spaggiari, G.; Fornari, R. Low Temperature Deposition of Bifacial CIGS Solar Cells on Al-Doped Zinc Oxide Back Contacts. *Applied Surface Science* **2017**, *412*, 52–57. <https://doi.org/10.1016/j.apsusc.2017.03.242>.
- (7) Yu, Z. (Jason); Leilaoui, M.; Holman, Z. Selecting Tandem Partners for Silicon Solar Cells. *Nature Energy* **2016**, *1* (11), 1–4. <https://doi.org/10.1038/nenergy.2016.137>.
- (8) Hanna, G.; Jasenek, A.; Rau, U.; Schock, H. W. Influence of the Ga-Content on the Bulk Defect Densities of Cu(In,Ga)Se₂. *Thin Solid Films* **2001**, *387* (1–2), 71–73. [https://doi.org/10.1016/S0040-6090\(00\)01710-7](https://doi.org/10.1016/S0040-6090(00)01710-7).
- (9) Cao, Q.; Gunawan, O.; Copel, M.; Reuter, K. B.; Chey, S. J.; Deline, V. R.; Mitzi, D. B. Defects in Cu(In,Ga)Se₂ Chalcopyrite Semiconductors: A Comparative Study of Material Properties, Defect States, and Photovoltaic Performance. *Advanced Energy Materials* **2011**, *1* (5), 845–853. <https://doi.org/10.1002/aenm.201100344>.
- (10) Larsson, F.; Nilsson, N. S.; Keller, J.; Frisk, C.; Kosyak, V.; Edoff, M.; Törndahl, T. Record 1.0 V Open-Circuit Voltage in Wide Band Gap Chalcopyrite Solar Cells. *Progress in Photovoltaics: Research and Applications* **2017**, *25* (9), 755–763. <https://doi.org/10.1002/pip.2914>.
- (11) Eisenbarth, T.; Unold, T.; Caballero, R.; Kaufmann, C. A.; Abou-Ras, D.; Schock, H.-W. Origin of Defects in CuIn_{1-x}Ga_xSe₂ Solar Cells with Varied Ga Content. *Thin Solid Films* **2009**, *517* (7), 2244–2247. <https://doi.org/10.1016/j.tsf.2008.10.142>.
- (12) Contreras, M. A.; Mansfield, L. M.; Egaas, B.; Li, J.; Romero, M.; Noufi, R.; Rudiger-Voigt, E.; Mannstadt, W. Wide Bandgap Cu (In, Ga) Se₂ Solar Cells with Improved Energy Conversion Efficiency. *Progress in Photovoltaics: Research and Applications* **2012**, *20* (7), 843–850.

- (13) Muzzillo, C. P.; Mansfield, L. M.; Dehart, C.; Bowers, K.; Reedy, R. C.; To, B.; Noufi, R.; Ramanathan, K.; Anderson, T. J. The Effect of Ga Content on the Selenization of Co-Evaporated CuGa/In Films and Their Photovoltaic Performance. *2014 IEEE 40th Photovoltaic Specialist Conference, PVSC 2014* **2014**, 1649–1654. <https://doi.org/10.1109/PVSC.2014.6925236>.
- (14) Choi, J. H.; Kim, K.; Eo, Y.-J.; Park, J. H.; Gwak, J.; Ahn, S.-K.; Cho, A.; Ahn, S.; Cho, J.-S.; Shin, K.; Yoon, K.; Kong, S. H.; Yun, J.-H.; Yoo, J. Wide-Bandgap CuGaSe₂ Thin Film Solar Cell Fabrication Using ITO Back Contacts. *Vacuum* **2015**, *120*, 42–46. <https://doi.org/10.1016/j.vacuum.2015.06.016>.
- (15) Chirilă, A.; Reinhard, P.; Pianezzi, F.; Bloesch, P.; Uhl, A. R.; Fella, C.; Kranz, L.; Keller, D.; Gretener, C.; Hagendorfer, H.; Jaeger, D.; Erni, R.; Nishiwaki, S.; Buecheler, S.; Tiwari, A. N. Potassium-Induced Surface Modification of Cu(In,Ga)Se₂ Thin Films for High-Efficiency Solar Cells. *Nature Materials* **2013**, *12* (12), 1107–1111. <https://doi.org/10.1038/nmat3789>.
- (16) Gloeckler, M.; Sites, J. R. Band-Gap Grading in Cu(In,Ga)Se₂ Solar Cells. *Journal of Physics and Chemistry of Solids* **2005**, *66* (11), 1891–1894. <https://doi.org/10.1016/j.jpcs.2005.09.087>.
- (17) Kaufmann, C. A.; Caballero, R.; Unold, T.; Hesse, R.; Klenk, R.; Schorr, S.; Nichterwitz, M.; Schock, H.-W. Depth Profiling of Cu(In,Ga)Se₂ Thin Films Grown at Low Temperatures. *Solar Energy Materials and Solar Cells* **2009**, *93* (6), 859–863. <https://doi.org/10.1016/j.solmat.2008.10.009>.
- (18) Miyazaki, H.; Mikami, R.; Yamada, A.; Konagai, M. Cu (InGa) Se₂ Thin Film Absorber with High Ga Contents and Its Application to the Solar Cells. *Journal of physics and chemistry of solids* **2003**, *64* (9–10), 2055–2058.
- (19) Witte, W.; Kniese, R.; Eicke, A.; Powalla, M. Influence of the Ga Content on the Mo/Cu (In, Ga) Se₂ Interface Formation. In *2006 IEEE 4th World Conference on Photovoltaic Energy Conference*; IEEE, 2006; Vol. 1, pp 553–556.
- (20) Müller, J.; Nowoczin, J.; Schmitt, H. Composition, Structure and Optical Properties of Sputtered Thin Films of CuInSe₂. *Thin Solid Films* **2006**, *496* (2), 364–370.
- (21) Moreau, A.; Insignares-Cuello, C.; Escoubas, L.; Simon, J.-J.; Bermúdez, V.; Pérez-Rodríguez, A.; Izquierdo-Roca, V.; Ruiz, C. M. Impact of Cu–Au Type Domains in High Current Density CuInS₂ Solar Cells. *Solar Energy Materials and Solar Cells* **2015**, *139*, 101–107. <https://doi.org/10.1016/j.solmat.2015.03.008>.
- (22) Wang, M.; Hossain, M. A.; Choy, K.-L. Effect of Sodium Treatment on the Performance of Electrostatic Spray Assisted Vapour Deposited Copper-Poor Cu(In,Ga)(S,Se)₂ Solar Cells. *Scientific Reports* **2017**, *7* (1), 1–10. <https://doi.org/10.1038/s41598-017-07027-9>.
- (23) James, B. A.; Adam, B.; Moores, J. Research Collection. **2004**. <https://doi.org/10.3929/ethz-a-010782581>.
- (24) Rincón, C.; Ramirez, F. J. Lattice Vibrations of CuInSe₂ and CuGaSe₂ by Raman Microspectrometry. *Journal of Applied Physics* **1992**, *72* (9), 4321–4324.
- (25) Fraga, D.; Stoyanova Lyubenova, T.; Martí, R.; Calvet, I.; Barrachina, E.; Carda, J. B. Effect of Alkali Doping on CIGS Photovoltaic Ceramic Tiles. *Solar Energy* **2017**, *147*, 1–7. <https://doi.org/10.1016/j.solener.2017.03.033>.
- (26) Insignares-Cuello, C.; Broussillou, C.; Bermúdez, V.; Saucedo, E.; Pérez-Rodríguez, A.; Izquierdo-Roca, V. Raman Scattering Analysis of Electrodeposited Cu(In,Ga)Se₂ Solar Cells: Impact of Ordered Vacancy Compounds on Cell Efficiency. *Appl. Phys. Lett.* **2014**, *105* (2), 021905. <https://doi.org/10.1063/1.4890970>.
- (27) Cuevas, A. The Recombination Parameter J₀. *Energy Procedia* **2014**, *55*, 53–62. <https://doi.org/10.1016/j.egypro.2014.08.073>.

- (28) Raghuwanshi, M.; Cadel, E.; Pareige, P.; Duguay, S.; Couzinie-Devy, F.; Arzel, L.; Barreau, N. Influence of Grain Boundary Modification on Limited Performance of Wide Bandgap Cu(In,Ga)Se₂ Solar Cells. *Appl. Phys. Lett.* **2014**, *105* (1), 013902. <https://doi.org/10.1063/1.4890001>.
- (29) Higuchi, T.; Usami, N.; Minemoto, T. Effect of Ga Content and Growth Temperature on Cu(In,Ga)Se₂ Thin Film Deposited on Heat-Resistant Glass Substrates. *physica status solidi c* **2013**, *10* (7–8), 1035–1037. <https://doi.org/10.1002/pssc.201200833>.
- (30) Baier, R.; Lehmann, J.; Lehmann, S.; Rissom, T.; Alexander Kaufmann, C.; Schwarzmann, A.; Rosenwaks, Y.; Lux-Steiner, M. Ch.; Sadewasser, S. Electronic Properties of Grain Boundaries in Cu(In,Ga)Se₂ Thin Films with Various Ga-Contents. *Solar Energy Materials and Solar Cells* **2012**, *103*, 86–92. <https://doi.org/10.1016/j.solmat.2012.04.002>.

Figures

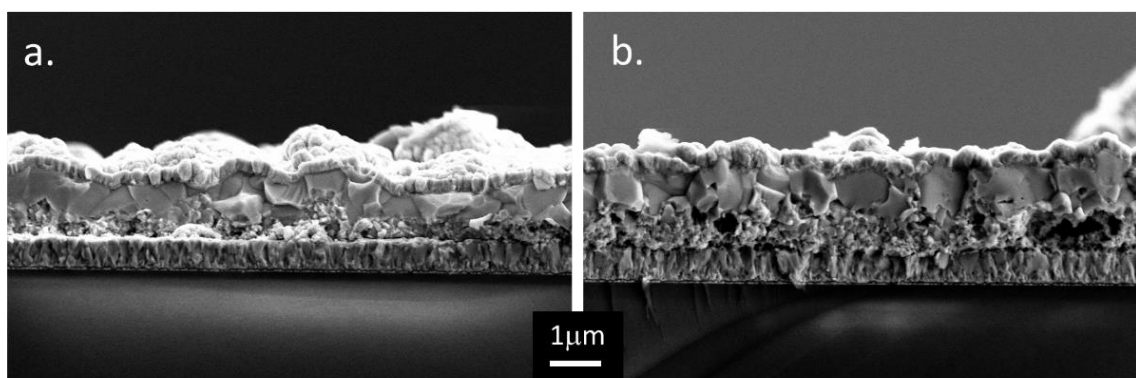


Figure 1. SEM images of the cross-section in samples #1 (a) and sample #2 (b) with a 10K magnification.

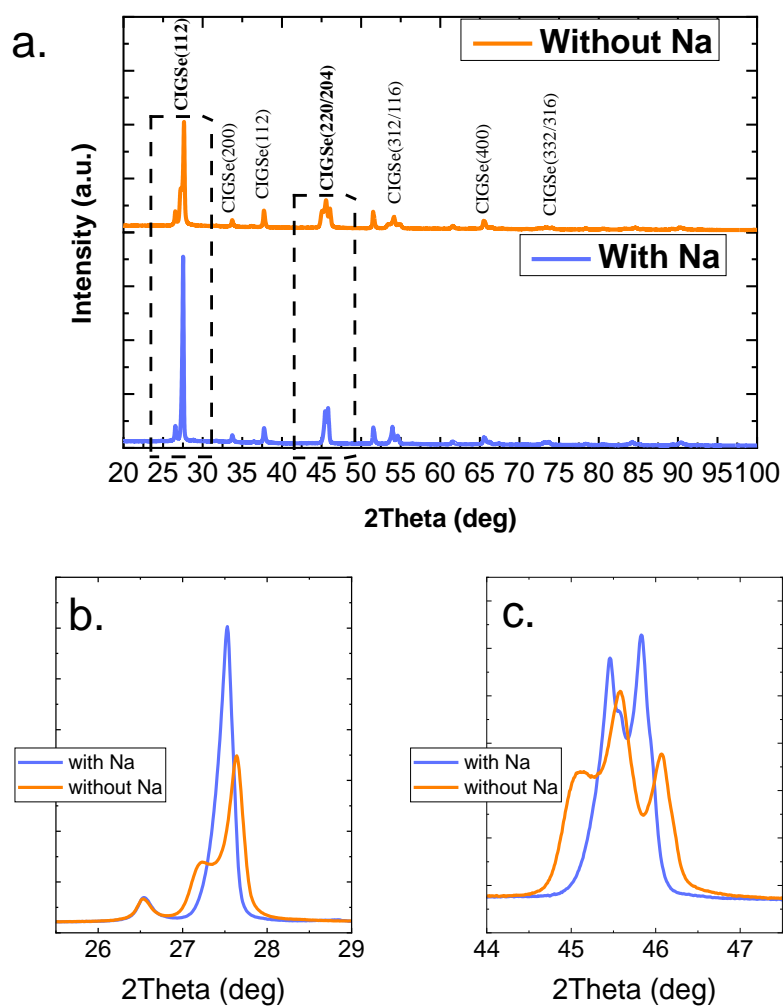


Figure 2. X-Ray Diffraction analysis of sample #1 and sample #2. Overview (a); 112 peak (b); 220/240 peaks (c).

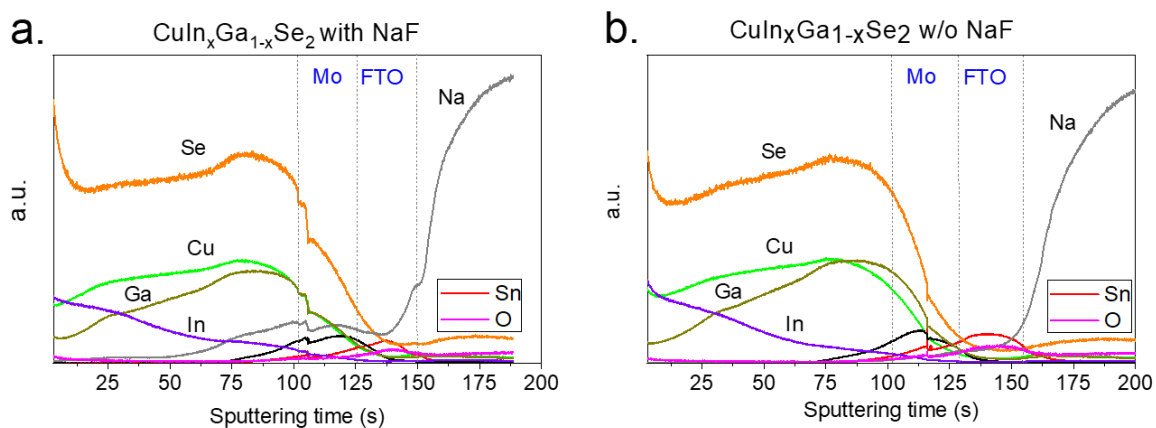


Figure 3. Depth composition profiles of sample #1 (a) and sample #2 (b) determined by a Glow Discharge Optical Emission Spectrometry analysis.

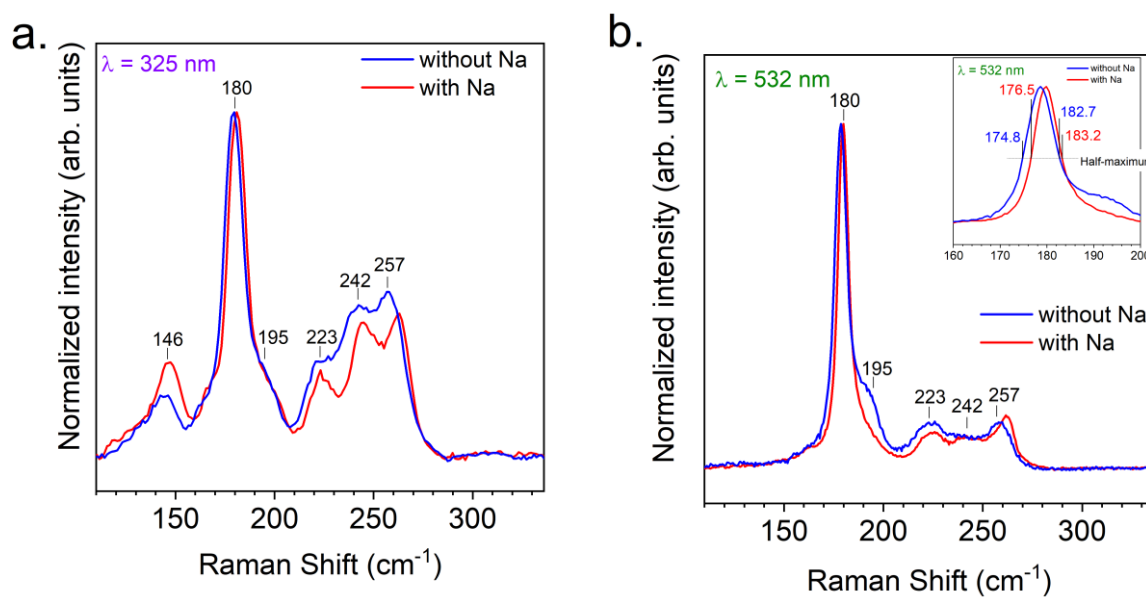
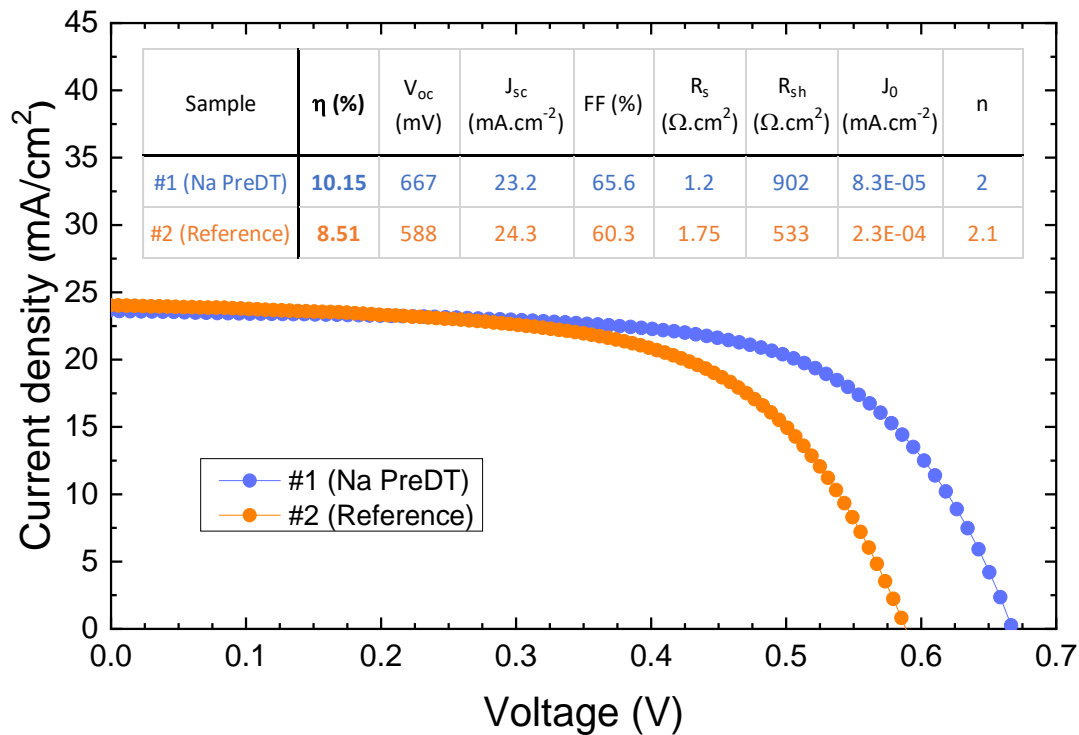


Figure 4. Raman spectra of sample #1 and sample #2 obtained using the 325nm (a) and the 532nm excitation wavelengths (b).

Table 1. Summary of the photovoltaic properties of wide bandgap CIGSe solar cells as reported in relevant references, and compared to the record device from this work.

Ref	GIG [%] or E_g [eV]	Substrate	V_{oc} [mV]	J_{sc} [$\text{mA}\cdot\text{cm}^{-2}$]	FF [%]	Eff (no ARC) [%]
[²⁸]	67%	Mo	750	21	70	11
[²⁹]	69%	Mo	633	13.7	57.3	4.97
[³⁰]	76%	Mo	718	13.1	51	4.8
[10]	1.70eV	Mo	1003	15.8	67.1	10.7
[12]	1.44eV	Mo	813	26.9	72.2	15.8
[13]	70%	Mo	643	25.9	73.2	12.2
[14]	1.65eV	ITO	780	12.8	50.6	5.0
This Work	68% and 1.41eV	FTO	667	23.2	65.5	10.15

**Figure 5.** Current Voltage curves under illumination and diode parameters for sample #1 (Na-PreDT) and sample #2 (Reference).

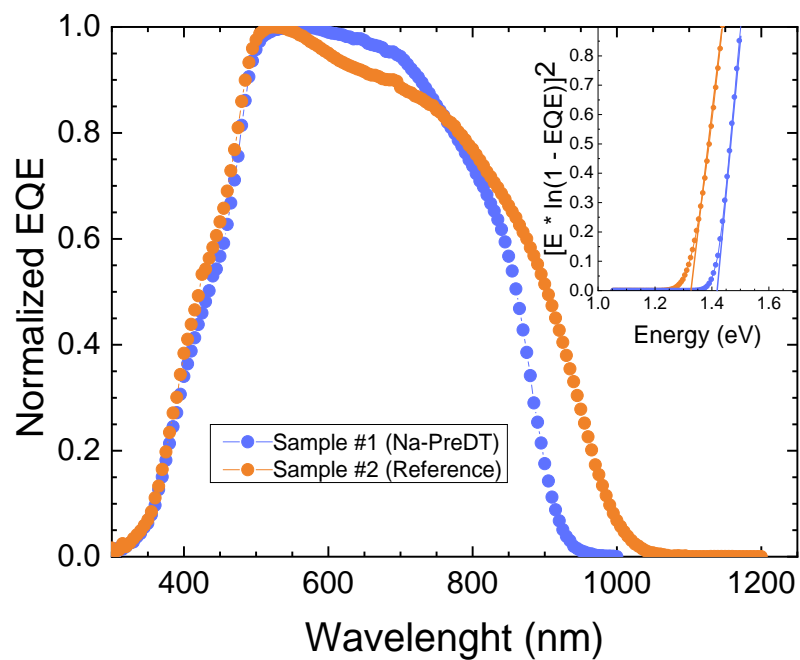


Figure 6. Compared Normalized External Quantum Efficiency of sample #1 and sample #2.

Inset: bandgap determination plot $h\nu \times \ln(1 - EQE)^2$ against $h\nu$.

Supporting Information

Over 10% Efficient Wide Bandgap CIGSe Solar Cells on Transparent Substrate with Na Pre-Deposition Treatment

Mohamed Ould Salem, Robert Fonoll, Sergio Giraldo, Yudania Sanchez, Marcel Placidi, Victor Izquierdo-Roca, Claudia Malerba, Matteo Valentini, Diouldé Sylla, Angelica Thomère, Dah Ould Ahmedou, Edgardo Saucedo, Alejandro Pérez-Rodríguez, and Zacharie Jehl Li-Kao

Substrate transparency and possible improvements

Experimental optical transmission of MoSe₂ films on SLG/FTO with and without Na-PreDT, compared with a bare FTO film and an FTO film with a 15nm Mo layer (before selenization). While a certain level of transparency is achieved (a median of approximately 40% in over the whole CIGSe absorption range), a significant room for improvement still exists in that regard.

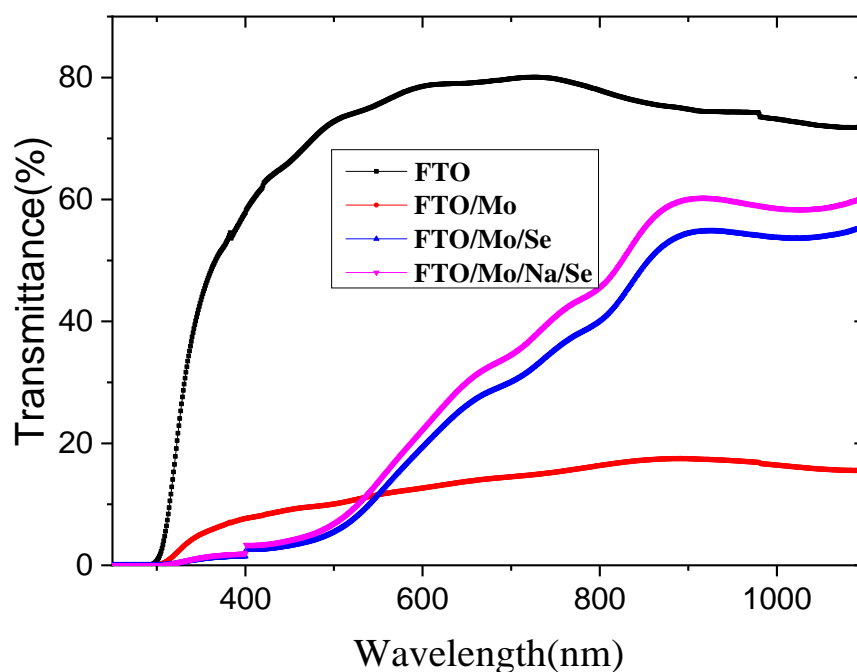


Figure S 1 Experimental optical transmission for different substrate configurations.

Compared modeled absorption and transmission of a SLG/FTO(300nm)/MoSe₂(30nm) stack, and a SLG/FTO(300nm)/MoO₃(30nm) stack. The latter shows significantly more transparency, and represents a pathway to follow on further improvement of the device's properties.

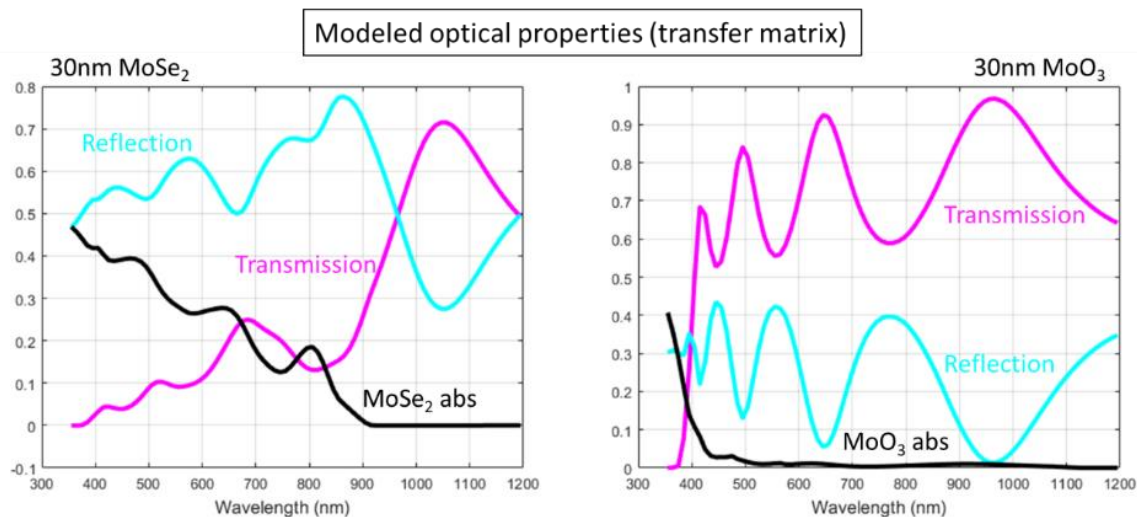


Figure S 2 Modeled optical transmission, reflection and layer absorption compared between a SLG/FTO/MoSe₂ stack (left) and SLG/FTO/MoO₃ stack (right).

Solar cells statistics

The figure below represent the photovoltaic parameters of various solar cells fabricated in condition similar to sample #1 and sample #2 in the. One can note that the J_{sc} values are, in average, even lower for sample #2 than for sample #1. Combined with the much wider data spread for sample #2, this is also consistent with a poor crystalline quality and reproducibility of the CIGSe growth in the absence of the alkaline element. In the manuscript, we decided to report on record cells only.

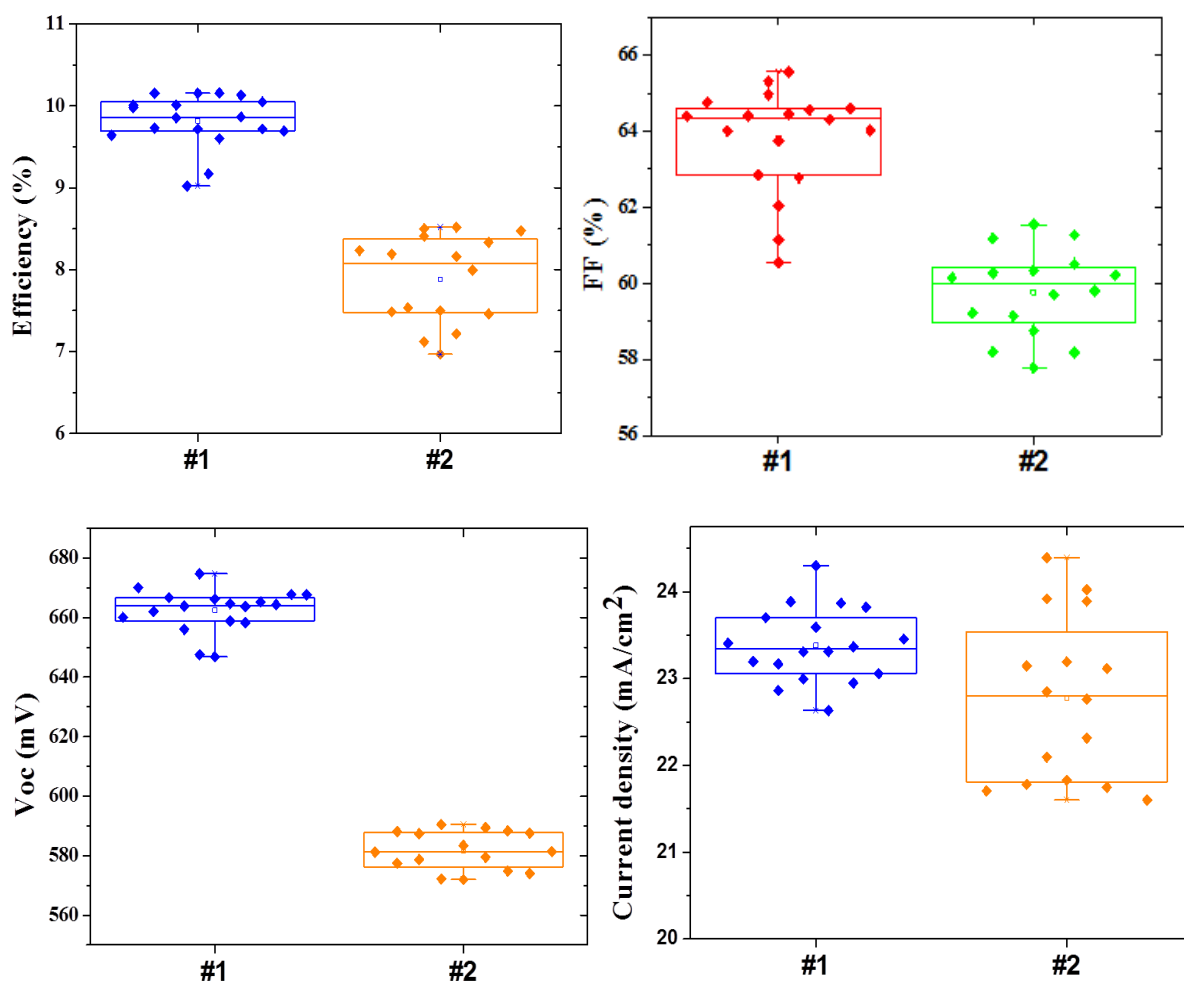


Figure S 3 Statistic distribution of the photovoltaic parameters